A Generalized Domain-Decomposition Stochastic FDTD Technique for Complex Nanomaterial and Graphene Structures

Nikolaos V. Kantartzis[1], Theodoros T. Zygiridis[2], Christos S. Antonopoulos[1], and Theodoros D. Tsiboukis[1]

[1]Dept. of Electrical & Computer Eng., Aristotle Univ. of Thessaloniki, 54124 Thessaloniki, Greece, kant@auth.gr
[2]Dept. of Informatics & Telecommunications Eng., Univ. of Western Macedonia, 50100 Kozani, Greece, tzygiridis@uowm.gr

The systematic and rigorous design of realistic nanocomposite applications and finite graphene setups with arbitrary media uncertainties is presented in this paper via a 3-D covariant/contravariant stochastic finite-difference time-domain method. The novel algorithm employs extra nodes according to a convex combination of all available spatial increments and develops a robust domain-decomposition scheme along with the pertinent Lagrange multipliers to significantly reduce the computational overhead. In this manner, the mean value and standard deviation of field components are calculated in a single run, which is further accelerated through graphics processor units and parallel programming. The profits of the proposed algorithm are certified by various nanoscale components with demanding statistical material variations.

***Index Terms*—Carbon compounds, computational electromagnetics, finite difference methods, nanomaterials, stochastic processes.**

I. Introduction

STOCHASTIC media problems addressing nanoscale devices or graphene arrangements with random constitutive parameters, have gained notable recognition [1]-[3]. Typically, these cases are studied by the Monte-Carlo (MC) method, which may offer sufficient results. Nevertheless, its slow convergence requires a large amount of stochastic data implementations, thus generating excessive system burdens. To mitigate this shortcoming, several effective schemes have been presented [4], [5]. In the former, a stochastic finite-difference time-domain (S-FDTD) method has been discussed for biological setups in Cartesian coordinates. Notwithstanding its obvious advantages, though, there are yet diverse concerns to be resolved, like the artificial dispersion errors and the correct manipulation of arbitrary media interfaces, as in the vicinity of electrically-large nanostructured configurations.

In this paper, a generalized 3-D S-FDTD method is introduced for the reliable analysis of stochastic non-uniformities in nanomaterial and finite graphene applications, due to the fabrication process. The new method is formulated by a covariant/contravariant curvilinear concept, which can precisely handle statistical electric permittivity, magnetic permeability, and losses. Based on auxiliary nodes at media interfaces, the curvilinear scheme leads to the optimal stencil through a weighted convex combination of all possible candidates and allocates fields on a dual mesh with subwavelength resolution. Also, wherever necessary the domain is divided into smaller subdomains, associated via Lagrange multipliers for the equivalent surface currents. Hence, the variance of field components is obtained at a much lesser computational time, as compared to the MC-FDTD approach, while extra acceleration is attained by graphical processor units (GPUs). The prior merits are effectively verified in terms of realistic nanocomposite setups.

II. Curvilinear Domain-Decomposition S-FDTD Schemes

Assume a coordinate system, where any vector can be expressed via the covariant $\{\mathbf{u}_1, \mathbf{u}_2, \mathbf{u}_3\}$ or the contravariant $\{\mathbf{u}^1, \mathbf{u}^2, \mathbf{u}^3\}$ base. So, electric **E** and magnetic **H** fields have a set of covariant (e_1, e_2, e_3), (h_1, h_2, h_3) or contravariant (e^1, e^2, e^3), (h^1, h^2, h^3) components. Also, every component $f_{i,j,k}$ inside a cell of volume V is given by

$$\overline{f}_{i,j,k}(t) = V^{-1} \iiint_V p(\varepsilon,\mu) f(\mathbf{r},t) dV \,, \tag{1}$$

with $p(\varepsilon, \mu)$ functions of the statistically-varying media constitutive parameters and **r** the position vector. Thus, spatial derivatives

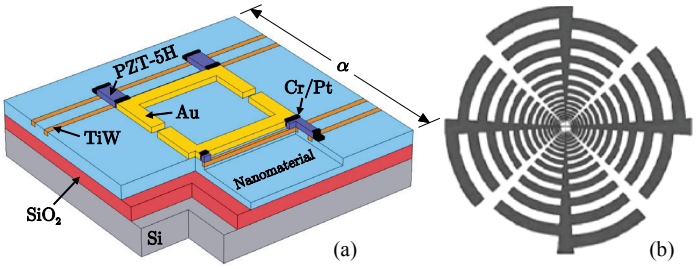

Fig. 1. (a) A reconfigurable nanomaterial-based device with four titanate (PZT-5H) actuators, two gold (Au) gripping arms, and a silicon (Si) substrate, and (b) top-view of a planar graphene (shaded area) circular-toothed log-periodic nanoantenna.

can be calculated by a set of new polynomials $Q_s(\mathbf{r},t)$, as

$$\partial_s f(\mathbf{r},t) = Q_s(\mathbf{r},t) + O[(\Delta s)^{q+1}] \,, \tag{2}$$

where s indicates the axis direction and Δs the spatial step. The key idea of the proposed $(2q-1)$th-order schemes is the weighted convex combination of all candidate stencils that yields rigorous reconstructions of $Q_s(\mathbf{r},t)$. Resolving the actual position of the respective nodes, these polynomials can be acquired by

$$Q_s(\mathbf{r},t) = \sum_{v=0}^{q-1} \frac{b_v^s}{\sum_{\tau=0}^{q-1} b_\tau^s} A_{v,s}(\mathbf{r},t) \,, \tag{3}$$

with b weighting coefficients and $A_{v,s}(\mathbf{r},t)$ interpolating polynomials for the highly-fluctuating stochastic uncertainties. Moreover, time update is conducted by a modified leapfrog scheme that preserves the electromagnetic energy. Hence, a non-oscillatory behavior is accomplished, unlike other schemes with two-point approximations. These enhanced stencils are obtained through

$$\{L_\delta\}_{u_2}^{q-1} = \left\{ f\big|_{i,j-\delta+q/2,k}^{n}, f\big|_{i,j-\delta+3q/2,k}^{n}, \ldots, f\big|_{i,j+\delta-q/2,k}^{n} \right\}, \tag{4}$$

for $\delta = 0,1,\ldots,q\text{-}1$ and along e.g. the u_2 direction in the domain.

To derive the stochastic technique, the general operator $\mathcal{R}$ (representing the mean value M or variance σ^2) is applied to the optimized FDTD equations. For instance, the e^1 component reads

$$\begin{aligned}\mathcal{R}\left\{e_1\big|_{i+1/2,j,k}^{n+1}\right\} = \mathcal{R}\Bigg\{ & C_a e_1\big|_{i+1/2,j,k}^{n+1} \\ & + \frac{C_b}{g^{1/2}\Delta u_2}\left(h^3\big|_{i+1/2,j+1/2,k}^{n+1/2} - h^3\big|_{i+1/2,j-1/2,k}^{n+1/2} + \zeta_{e_{12}}\big|_{i+1/2,j,k}^{n+1/2} \right) \\ & - \frac{C_b}{g^{1/2}\Delta u_3}\left(h^2\big|_{i+1/2,j,k+1/2}^{n+1/2} - h^2\big|_{i+1/2,j,k-1/2}^{n+1/2} + \zeta_{e_{13}}\big|_{i+1/2,j,k}^{n+1/2} \right) \Bigg\}, \end{aligned} \tag{5}$$

with g the Jacobian determinant of g_{lm} metrics (l, m = 1,2,3) and coefficients C referring to random media. For infinite boundaries,

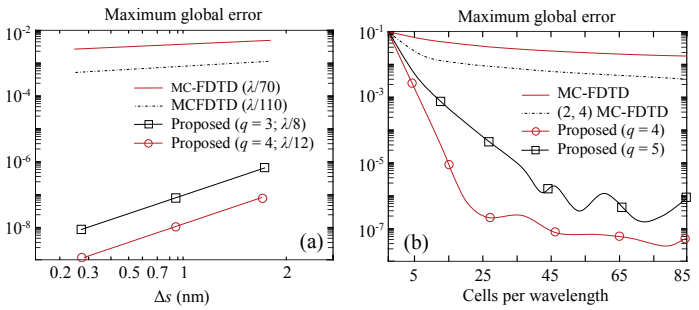

Fig. 2. Maximum global error versus (a) spatial step and (b) spatial resolution.

a reformed convolutional perfectly matched layer (CPML) is employed, whose covariant ζ_{12} and ζ_{13} components are given by

$$\mathcal{R}\left\{\zeta_{12}\big|_{i+1/2,j,k}^{n+1/2}\right\}=\mathcal{R}\left\{Y_1\,\zeta_{12}\big|_{i+1/2,j,k}^{n-1/2}+D_1\left(h^3\big|_{i+1/2,j+1/2,k}^{n+1/2}-h^3\big|_{i+1/2,j-1/2,k}^{n+1/2}\right)\right\}, \quad (6)$$

$$\mathcal{R}\left\{\zeta_{13}\big|_{i+1/2,j,k}^{n+1/2}\right\}=\mathcal{R}\left\{Y_2\,\zeta_{13}\big|_{i+1/2,j,k}^{n-1/2}+D_2\left(h^2\big|_{i+1/2,j,k+1/2}^{n+1/2}-h^2\big|_{i+1/2,j,k-1/2}^{n+1/2}\right)\right\}, \quad (7)$$

where Y_s, D_s contain CPML traits along the covariant s direction. For the contravariant components in (5), we employ a metrics interpolation which involves their covariant counterparts toward the other two directions. Also, via first-order approximations in the Taylor series expansion, it is proven that the M and σ^2 values of a $f(y_1, y_2,\ldots, y_n)$ function with random variables $y_1, y_2,\ldots, y_n$, are

$$M\{f(y_1,y_2,\ldots,y_n)\}\approx f(m_{y_1},m_{y_2},\ldots,m_{y_n}), \quad (8)$$

$$\sigma^2\{f\}\approx\sum_{i=1}^{n}\sum_{j=1}^{n}\partial_{y_i}f\,\partial_{y_j}fM\left\{(y_i-m_{y_i})(y_j-m_{y_j})\right\}, \quad (9)$$

for m_{y1}, $m_{y2},\ldots, m_{yn}$ the mean values of $y_1, y_2,\ldots, y_n$. These random variables are the six electric and magnetic components, the media constitutive parameters and the loss terms. To minimize the system overhead, the 3-D space is separated into subdomains via an automatic partition scheme, i.e. division into 2 central, 6 face, and 6 edge non-overlapping areas. For field continuity at the interfaces, a Lagrange multipliers process is applied. Finally, in regions of mild uncertainties our scheme combines time-domain free-space Green's functions [6]-[8] and surface impedance boundary conditions. This approach and (1)-(4) forms achieve a greatly improved dispersion relation (compared to the typical $\mathcal{D}_{\text{FDTD}}$ one)

$$\sin^2\left(\omega\Delta t/2\right)/\mathcal{D}_{\text{FDTD}}\approx 62(\Delta s)^{(3q-1)/7}/[3^{q+1}(\mu\varepsilon)^{1/2}], \quad (10)$$

as deduced from the maximum global error results of Fig. 2. Note that the grid and time-step size are determined via the generalized Courant stability condition, which employw the g_{lm} metrics [4].

III. Numerical Results – Conclusions

To validate the novel algorithm, a set of real-world nanoscale setups, truncated by an 8-cell-thick CPML, is examined. First, we analyze the reconfigurable device (α = 14 μm) of Fig. 1(a), which comprises a 1.5 μm silicon (Si) substrate, a 0.8 μm silicon oxide (SiO_2) isolation layer, and a 0.7 μm nanomaterial (Nanotech™ 24). Two pairs of titanium tungsten (TiW) electrodes are considered, while four zirconium titanium (PZT-5H) and two gold (Au) grippers complete the structure. The stochastic parameters of the structure are m_ε = 4.2, $\sigma\{\varepsilon\}$ = 0.1 and the domain is discretized into a 94×94×62 grid, unlike the 674×674×458 mesh of the MC-FDTD one. Figure 3 shows the S_{21}-parameter and return loss of the device, revealing the superior accuracy of the featured method, just for a single-run realization. Next, the circular-toothed log-periodic nanoantenna with the graphene pattern of Fig. 1(b) is

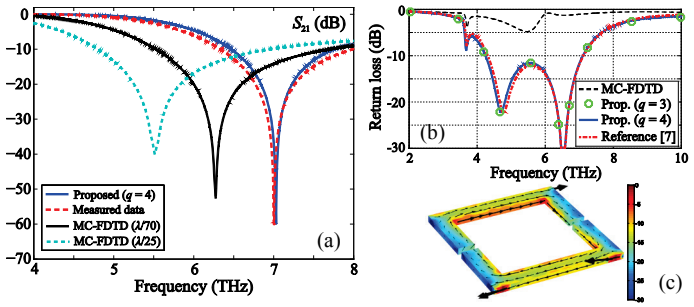

Fig. 3. (a) Magnitude of the S_{21}-parameter, (b) rerurn loss, and (c) surface current density snapshot at t = 391 nsec for the nanomaterial-based device.

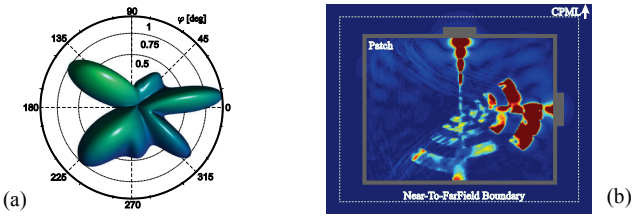

Fig. 4. (a) Mean value of the radiation pattern across the z-plane and (b) standard deviation of the current distribution for the circular-toothed graphene antenna.

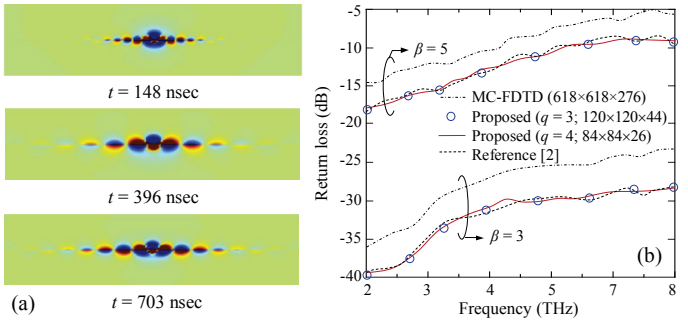

Fig. 5. (a) Distribution of the normal to the graphene E_y surface plasmon polariton (mean value) at three time instants and (b) return loss (mean value) for various β.

explored. The angle of the teeth is 75° and their number, β, is variable. Graphene is realized via the popular Kubo formula and its uncertainties are m_ε = 3.5, $\sigma\{\varepsilon\}$ = 0.7. Several stochastic quantities are given in Figs 4 and 5(a), whereas Fig. 5(b) proves the efficiency of our technique for this highly curved application. Finally, it is stressed that the GPU simulation of both problems has been more than 100 faster than the MC-FDTD approach.

References

[1] G. Shvets and I. Tsukerman, *Plasmonics and Plasmonic Metamaterials*. Singapore: World Scientific Publishing, 2012.

[2] S. Cruciani, V. De Santis, F. Maradei, and M. Feliziani, "Circuit-oriented solution of Drude dispersion relations by the FD²TD method," *IEEE Trans. Magn.*, vol. 50, no. 2, art. no. 6749202, 2014.

[3] C. Classen, B. Bandlow, and R. Schuhmann, "Local approximation based on material averaging approach in the finite integration technique," *IEEE Trans. Magn.*, vol. 48, no. 6, art. no. 6202772, 2012.

[4] T. Tan, A. Taflove, and V. Backman, "Single realization stochastic FDTD for weak scattering waves in biological random media," *IEEE Trans. Antennas Propag.*, vol. 61, no. 2, pp. 818–828, Feb. 2013.

[5] L. Codecasa and L. Di Rienzo, "Stochastic finite integration technique formulation for electrokinetics," *IEEE Trans. Magn.*, vol. 50, no. 2, art. no. 7014104, Feb. 2014.

[6] G. Peng, R. Dyczij-Edlinger, and J.-F. Lee, "Hierarchical methods for solving matrix equations from TVFEMs for microwave components," *IEEE Trans. Magn.*, vol. 35, no. 3, pp. 1474–1477, May 1999.

[7] X. Wang, Z. Peng, K.-H. Lim, and J.-F. Lee, "Multisolver domain decomposition method for modeling EMC effects on large air platforms," *IEEE Trans. Electromagn. Compat.*, vol. 54, no. 2, pp. 375–388, Feb. 2012.

[8] C. Richter, S. Schops, and M. Clemens, "GPU acceleration of finite difference schemes used in coupled electromagnetic/thermal field simulation," *IEEE Trans. Magn.*, vol. 49, no. 2, pp. 1649–1652, May 2013.